Journal of Applied Physics

Engineering the carrier lifetime and switching speed in Si-based mm-wave photomodulators

Cite as: J. Appl. Phys. **132**, 233102 (2022); https://doi.org/10.1063/5.0128234
Submitted: 01 October 2022 • Accepted: 25 November 2022 • Published Online: 16 December 2022
Published open access through an agreement with JISC Collections

I. R. Hooper, E. Khorani, X. Romain, et al.

Journal of Applied Physics ARTICLE scitation.org/journal/jap

Engineering the carrier lifetime and switching speed in Si-based mm-wave photomodulators

Cite as: J. Appl. Phys. **132**, 233102 (2022); doi: 10.1063/5.0128234
Submitted: 1 October 2022 · Accepted: 25 November 2022 ·
Published Online: 16 December 2022

I. R. Hooper,[1,a)] E. Khorani,[2] X. Romain,[2] L. E. Barr,[1] T. Niewelt,[2,3] S. Saxena,[1] A. Wratten,[2] N. E. Grant,[2] J. D. Murphy,[2] and E. Hendry[1]

AFFILIATIONS

[1]Department of Physics and Astronomy, University of Exeter, Stocker Road, Exeter EX4 4QL, United Kingdom
[2]School of Engineering, University of Warwick, Coventry CV4 7AL, United Kingdom
[3]Fraunhofer Institute for Solar Energy Systems ISE, Heidenhofstraße 2, 79110 Freiburg, Germany

[a)]**Author to whom correspondence should be addressed:** i.r.hooper@exeter.ac.uk

ABSTRACT

For a diverse range of semiconductor devices, the charge carrier lifetime is an essential characteristic. However, the carrier lifetime is difficult to control, as it is usually determined by a variety of recombination processes. For indirect bandgap materials, it is well known that effective carrier lifetimes can be improved by passivating the surface, effectively extinguishing surface-related recombination processes. However, for some applications, such as photomodulators for sub-infrared radiation, it is beneficial to tailor lifetimes to specific values, in this particular case trading off between photo-efficiency and switching speed. In this paper, we design a new type of silicon-based metamaterial with a tunable electron–hole lifetime. By periodically patterning a dielectric surface passivation layer, we create a metamaterial whereby the filling fraction of passivated relative to unpassivated areas dictates the effective charge carrier lifetime. We demonstrate tunable lifetimes between 200 μs and 8 ms in a 670 μm thick Si wafer, though in principle our approach allows one to generate any lifetime between the fully passivated and unpassivated limits of a bulk semiconductor. Finally, we investigate the application of these metamaterials as photomodulators, finding switching times that depend upon both the photoexcitation intensity, wafer thickness, and the carrier lifetime.

I. INTRODUCTION

Semiconductors are ubiquitous in modern technology and find applications in electromagnetic modulators,[1–3] photovoltaics,[4] and photoelectrochemical cells,[5] in addition to their established use in the electronics industry. The dynamics of charge carriers (electrons and holes) determine their suitability for a given application, and the charge carrier lifetime is one important parameter in describing these dynamics.

The focus for many applications is on maximizing lifetime. This is particularly important for silicon photovoltaics, where a longer lifetime of the photoexcited charge carriers results in a correspondingly longer diffusion length, and hence a higher efficiency solar cell.[6] Indirect bandgap semiconductors (e.g., Si, Ge) have intrinsically long bulk charge carrier lifetimes due to the lack of radiative recombination, so their lifetime is mainly limited by recombination at defects in the bulk of the material or at surfaces.[7] Modern materials can be made defect-lean, hence surface recombination often limits lifetimes in practice. Various surface "passivation" schemes have been devised[8–10] to reduce, and largely eliminate, recombination at the surfaces, allowing effective charge carrier lifetimes of as high as 0.5 s to be achieved on high resistivity silicon wafers.[11] For moderate doping, effective lifetimes of 1–30 ms are more usually achieved due to the limitations of intrinsic (mostly Auger) recombination.[12]

However, there are also applications which would benefit from a tuneable carrier lifetime, and this is particularly important when designing modulators for the manipulation of sub-IR electromagnetic radiation. In these photomodulators, incident light with photon energies higher than or equal to the semiconductor bandgap change the conductivity, altering the reflection/transmission of the longer wavelength radiation from/through the semiconductor.[1–3,13] The conductivity can be changed locally with inhomogeneous illumination, allowing a beam to be steered

or focused,[14–17] giving similar functionality to so-called "reconfigurable" and "programmable" metasurfaces at GHz frequencies.[18–22] Such modulation effects can also be used in single-pixel imaging schemes at these frequencies.[23–26] Reviews of the current state-of-the-art in mm-wave and THz modulators can be found in Refs. 1–3.

While a long charge carrier lifetime increases the efficiency of photomodulation, it also limits the operational switching speed.[13] Longer carrier lifetimes can also lead to significant lateral diffusion of the charge carriers and correspondingly lower resolutions in imaging.[26] Ideally, one would like to tune the carrier lifetime to match the speed of a particular application, thereby optimizing the benefits of longer carrier lifetimes without excessively limiting the switching speeds. While very short effective lifetimes ($\lesssim 10\,\mu$s) are common for unpassivated wafers, and high-quality surface passivation results in long carrier lifetimes ($\gtrsim 10$ ms),[13] there is a large intermediate region of effective lifetimes which is difficult to reach. Though there have been some previous efforts to modify the charge carrier lifetime,[27] no systematic method has been developed to enable precise tuning of the lifetime to reach arbitrary values between the intrinsic and unpassivated limits.

In this paper, by patterning a passivation layer, we create a metamaterial in which the filling fraction of unpassivated to passivated areas dictates the effective charge carrier lifetime (Fig. 1). Here, we passivate the surface using Al_2O_3 grown by atomic layer deposition (ALD),[28–30] but note that other dielectric passivating layers such as thermally grown SiO_2 could also be used. Finite element simulations are used to predict the filling fractions required to give effective lifetimes ranging from 100 μs up to several ms in a 670 μm thick wafer. Nine designs with different filling fractions of unpassivated areas are subsequently realized on a single wafer via wet-chemical etching of the passivation layer using a photo-lithographic process. The effective charge carrier lifetime for each region is inferred from the transmission switching-dynamics of 321 GHz radiation through the wafer upon photoexcitation. The approach used is potentially applicable to other semiconductors, and, in principle, can be used to produce bespoke photomodulators for specific applications.

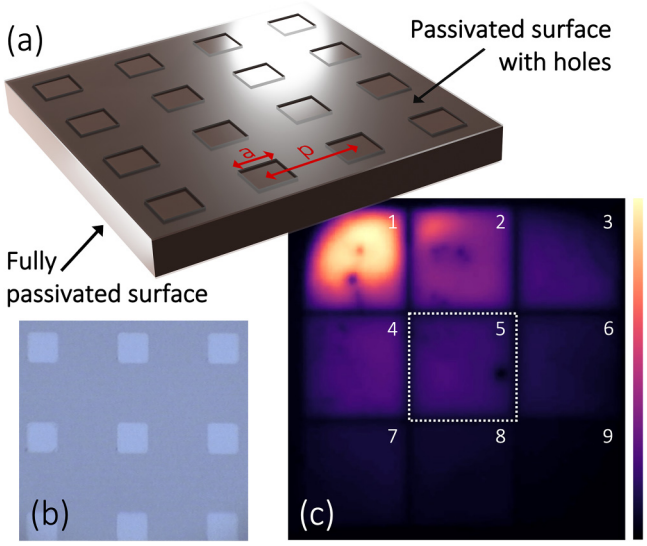

FIG. 1. To tailor the effective lifetime of charge carriers in a silicon wafer, we passivate the surfaces to effectively eliminate surface recombination, and then introduce an array (period *p*) of square holes (side length *a*) into the passivation layer on one surface to obtain the desired lifetime. Also shown is a microscope image of the patterned passivation layer (b), showing a 100 μm periodic array of holes in the passivation layer, and a photoluminescence image of the fabricated wafer (c), showing nine regions with different filling fractions of unpassivated holes. Each of the nine patterned regions is 2.5 cm square. Detailed analysis of the data for area 5 (white square) is described later in the paper, with the remainder within the supplementary material.

II. DESIGN PROCESS

A design process using COMSOL Multiphysics® is undertaken to determine the effect of incorporating a periodic array of holes in a surface passivation layer on the effective charge carrier lifetime of a silicon wafer. COMSOL Multiphysics® is a commercially available finite element method solver that, when coupled with the Semiconductor Module,[31] solves Poisson's equation alongside the continuity equations for the charge carriers. While it is a very general tool capable of modeling a vast array of semiconductor devices, here we use it to model the charge carrier distribution throughout a wafer as a function of time given surface and bulk carrier generation/recombination rates.

A square unit cell with a side length of 100 μm is chosen since it is significantly smaller than both the wavelength of radiation to be modulated and the carrier diffusion length (>500 μm for the resulting lifetimes), while being sufficiently large for ease of lithography. A 670 μm thick undoped Si wafer is modeled with a constant bulk lifetime of 50 ms using COMSOL's inbuilt Shockley–Read–Hall (SRH) recombination model. Note that in all cases the calculated effective lifetime is limited by surface recombination, so the chosen bulk lifetime of 50 ms is somewhat arbitrary—it simply needs to be much longer than the surface lifetime, though a value of 50 ms is reasonable for the very high-resistivity FZ wafers used in our experiments. The model also includes Auger and radiative recombination processes within the bulk of the wafer, though our modeling predicts that, for the effective lifetimes and photoexcitation intensities used in this study, the maximum carrier densities achieved within the wafer are below 10^{21} m^{-3}—densities at which one would expect Auger and radiative recombination to have little effect on the effective charge carrier lifetime.[12] As such, a bulk lifetime independent of the photoexcited carrier density is a good approximation.

The recombination at the surfaces is modeled using COMSOL's inbuilt SRH-based "trap-assisted surface recombination" physics. One surface is modeled as "fully passivated" with a surface recombination velocity (SRV) of 0.001 m s^{-1}. The majority of the second surface is described similarly, except for a square hole in the center of this passivated surface with a SRV of between 10 and 100 m s^{-1}, since the SRV of an unpassivated surface is expected to be within this range.[32] The model is then meshed with sufficient density close to the surfaces such that the large gradients in the

charge carrier density close to the surfaces as a result of surface recombination can be accurately represented.

A spatially dependent free-carrier generation rate describing photoexcitation upon the partially passivated surface is given by $A\exp(-\kappa_a z)$, where $\kappa_a = 4\pi n_i/\lambda$ is the absorption coefficient and $A = \kappa_a IT\lambda/hc$ corresponds to the density of electron–hole pairs generated at the illuminated surface (n_i is the imaginary part of the refractive index at wavelength λ, I is the intensity of the photoexciting light, z is the distance from the illuminated surface, and T is the fraction of the photoexciting light intensity that penetrates the interface). Unless otherwise stated, we model 20 W m^{-2} of 625 nm light incident upon the surface, with a Si refractive index of $n = n_r + n_i = 3.89 + 0.017i$. Note that the thickness of the passivating layers used in our experiments is sufficiently small that they are neglected in all modeling.

The steady-state charge carrier density profile throughout the modeling volume is calculated using COMSOL's stationary solver, with this subsequently being used as the initial condition for a time-dependent study with no generation rate, mimicking the switch-off dynamics after turning off a photoexciting source. For each time step, the carrier density within the volume is integrated, with the effective charge carrier lifetime corresponding to the time at which this value has reduced to 1/e of the steady-state value. This process is undertaken for a range of filling fractions of the holes in the passivation layer—the results are shown in Fig. 2. Note that the calculated effective charge carrier lifetime is largely independent of which surface is photoexcited—this will be discussed in more detail later. An equivalent plot for a 100 μm thick wafer is included in the supplementary material (Sec. 1) for comparison—the effective lifetimes are correspondingly shorter since the probability of an excess carrier diffusing to a surface is increased, but the range of lifetimes as a function of filling fraction is similar.

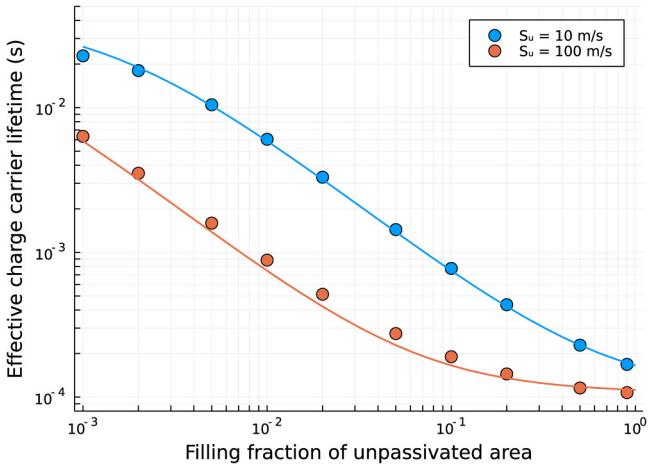

FIG. 2. Modeled effective charge carrier lifetime as a function of the filling fraction of unpassivated area within the passivation layer for a 670 μm thick wafer that is fully passivated on one surface and has a patterned passivation on the other. Results are shown for an SRV of the passivated areas of $S_p = 0.001$ m s^{-1}, and of the unpassivated holes, S_u, of 10 and 100 m s^{-1}. Symbols: COMSOL Multiphysics model. Lines: analytical model. See the main text for details.

To corroborate our numerical modeling, we also develop an analytical approach. The time-dynamics of the charge carrier profile within a wafer with surface recombination at each surface can be determined using the Fourier expansion method from the continuity equation alongside boundary conditions describing recombination at the surfaces.[33–35] The build-up / decay of carriers within the wafer is described by an infinite series of modes with associated time constants, τ_m,

$$\frac{1}{\tau_m} = \frac{1}{\tau_b} + \beta_m^2 D, \tag{1}$$

where D is the diffusion constant, τ_b is the bulk lifetime, and β_m are calculated from

$$\tan(\beta_m d) = \frac{\beta_m D(S_0 + S_1)}{\beta_m^2 D^2 - S_0 S_1}, \tag{2}$$

with S_0 and S_1 being the surface recombination velocities of the two surfaces. All higher order modes decay quickly, typically leaving the time constant of the fundamental mode to be identified as the effective lifetime of any excess carriers within the wafer.

We can calculate an effective SRV for our patterned surface passivations by using a linear combination of the SRVs of the passivated surface and unpassivated holes multiplied by their areal fractions,

$$S_{\text{eff}} = S_{\text{u}}\text{F} + S_{\text{p}}(1 - \text{F}), \tag{3}$$

where F is the filling fraction of holes in the passivation layer, and S_p and S_u are the SRVs of the passivated and unpassivated areas, respectively. Calculating S_{eff} as a function of filling fraction from Eq. (3), we can then introduce S_{eff} as S_0 in Eqs. (1)–(2) (with $D = 0.0017$ m^2 s^{-1}, $S_1 = 0.001$ m s^{-1}, and $d = 670\,\mu$m) to predict the effective lifetimes of a wafer with a patterned passivation. These are shown as lines in Fig. 2 and compare well with the results from the full COMSOL Multiphysics models.

One may notice that the effective carrier lifetime calculated from Eqs. (1)–(2) is independent of which surface of the wafer is photoexcited, and this is a result of neglecting the higher order decay modes. While this is a good approximation, when there is a large difference between the SRVs of the two surfaces differences in the effective lifetime become evident. This is the source of the small discrepancy between the COMSOL and analytical models, and it is discussed in more detail in the supplementary material (Sec. 5).

For a single surface with etched holes in the passivation layer, the results in Fig. 2 suggest that the effective charge carrier lifetime can be tuned over two orders of magnitude for filling fractions between 0.001 and 1. If both surfaces are patterned, the full range of carrier lifetimes between the fully passivated and unpassivated lifetimes would be achievable. For a 670 μm thick wafer, as studied here, this is expected to range from approx. 10 μs (with shorter lifetimes expected for thinner wafers) up to 10 s of ms (the bulk lifetime of the wafer).

For ease of fabrication, the minimum filling fraction for experimental study is chosen to be 0.01, corresponding to a hole side length of 10 μm. We then determined from Fig. 2 nine filling fractions of holes that would result in an approximately linear variation in lifetime between the nine etched regions on our wafer. Below, we describe the different fill fractions as areas 1–9, with area 1 having the smallest filling fraction of holes in the passivation layer and consequently the highest effective charge carrier lifetime.

III. FABRICATION

The patterned passivations are fabricated on a lowly doped monocrystalline Si wafer [float-zone, 10 kΩ cm, (100) orientation, 670 μm thick] that is initially cleaned in RCA-1 and RCA-2 solutions, followed by immersion in hydrofluoric acid (1%) for 60 s. The wafer is passivated using Al_2O_3 grown via plasma-enhanced ALD using a Veeco Fiji G2 ALD system. The chamber pressure is kept at 5 Pa, the plasma power at 300 W, and the bottom plate temperature at 200°C. Using a trimethylaluminum (TMA) precursor and O_2 plasma source, 200 cycles of ALD Al_2O_3 growth are conducted on both sides of the Si wafer. To protect the rear-side passivation during the etching process on the front-side, a hafnium oxide layer is deposited using a tetrakis(dimethylamido) hafnium (TDMA-Hf) precursor and an O_2 plasma source for 150 cycles. For charge activation and interfacial defect density reduction at the Al_2O_3–Si interfaces, and crystallization of the hafnium oxide protection layers, the wafer is annealed at 400°C for 30 min in air in a box furnace. The annealing temperature of 400°C is chosen as a compromise between activation of the surface passivation layers[36,37] and the detrimental effects of potential activation of unwanted bulk defects.[38,39]

For the front-side patterning, S1818 photoresist is spun at 5000 rpm for 30 s, followed by a soft bake at 115°C for 1 min. Using a custom-made photomask incorporating the nine square regions (each with a 2.5 cm side length) with different filling fractions of holes, the photoresist is exposed for 3 s in a soft contact mode with 100 μm mask-wafer separation using a Suss MicroTec BA8 Gen3 mask aligner. Following exposure, the photoresist is developed in MF319 solution for 45 s, followed by a rinse in de-ionized water. To protect the photoresist during wet etching of the Al_2O_3 layer, a hard bake at 130°C for 5 min is conducted following development. The structures are then etched in tetramethylammonium hydroxide (2% conc.) solution for 25 min. Post-development microscope images of each patterned area are shown in the supplementary material (Sec. 3).

In order to confirm the success of the etching process, photoluminescence (PL) images of the wafer are taken using a BT Imaging PL system (see Fig. 1). The PL intensity is related to the local carrier lifetime,[40] and a variation of the PL signal is clearly evident between the nine regions. Note that the black region in the upper left corner of area 1 is observed to have a significantly lower PL (and lifetime), resulting from manual handling of the wafer—this area is avoided during the mm-wave transmission measurements described in the following section. One can also observe small blemishes in the PL from the other regions resulting from imperfect processing. The imperfections introduce some degree of variability to our results compared to modeled predictions. Also note that the PL signal between the patterned regions reduces to close to the background level, indicating that there is little diffusion of charge carriers between them—even though the diffusion length for the longer lifetime regions can be as a long as a few mm, the unpassivated areas between them have much shorter lifetimes, essentially isolating the regions from each other.

IV. TIME-RESOLVED TRANSMISSION MEASUREMENTS AND EFFECTIVE LIFETIMES

The patterned Si wafer is mounted midway between a 321 GHz source[41] and detector[42] on a translation stage that allows the wafer to be positioned such that the GHz beam can pass through the center of each patterned region in turn. The wafer is mounted at normal incidence to the GHz beam, which has a diameter of approximately 5 mm (−3dB) at the wafer, with the patterned side facing the source. Two sheets of 3.5 mm ABS-ASF4 mm-wave absorber are placed either side of the wafer in order to detune any cavity resonances set up between the faces of the source, detector, and wafer.

A 623 nm high-power SOLIS LED from Thorlabs is placed 30 cm away from, and at a 45° angle to, the wafer, illuminating the patterned surface. This photoexciting optical beam is approximately 10 cm in diameter and centered over the GHz beam. The SOLIS lamp is driven using a Thorlabs DC2200 supply with variable intensity output up to a maximum of 764 W m^{-2} at the wafer position and is square-wave modulated with a period of 100 ms.

The signal from the detector is captured on a Siglent SDS2352X-E oscilloscope, triggered by the DC2200 supply, allowing the switch-on and switch-off dynamics of the transmission of the 321 GHz beam through the wafer to be recorded as the photoexciting optical pump light is modulated. This is undertaken for a range of intensities of the photoexciting source and for each patterned region on the wafer. The time-series data are smoothed[43] and normalized between the maximum and minimum values for each photoexcitation intensity to facilitate simple extraction of the intensity-dependent switching times. An example data set, from area 5 in the middle of the wafer, is shown in Fig. 3—equivalent data for the eight other patterned regions can be found in the supplementary material (Sec. 2).

We define the switch on and switch off times to be the time taken for the transmission to reduce/increase by $\Delta T\left(1-\frac{1}{e}\right)$, where ΔT is the steady-state change in transmission upon photoexcitation. Thus, the switch on time is given by $T_0-\Delta T\left(1-\frac{1}{e}\right)$ and the switch off time is given by $T_e+\Delta T\left(1-\frac{1}{e}\right)$, where T_0 and T_e are the transmitted intensities before photoexcitation and after prolonged photoexcitation (steady-state), respectively.

These times are extracted for each photoexcitation intensity and are shown in Fig. 4 for area 5. The low-injection (low photoexcitation intensity) switching time can be identified as the effective charge carrier lifetime, and this is indicated with a black dashed line. Also shown is the steady-state transmission upon photoexcitation (here, taken as the transmission just before the photoexciting source switches off, a time scale much longer than the switching dynamics), normalized to the measured signal without the wafer present. Similar plots can again be found in the supplementary material (Sec. 2) for the other patterned regions.

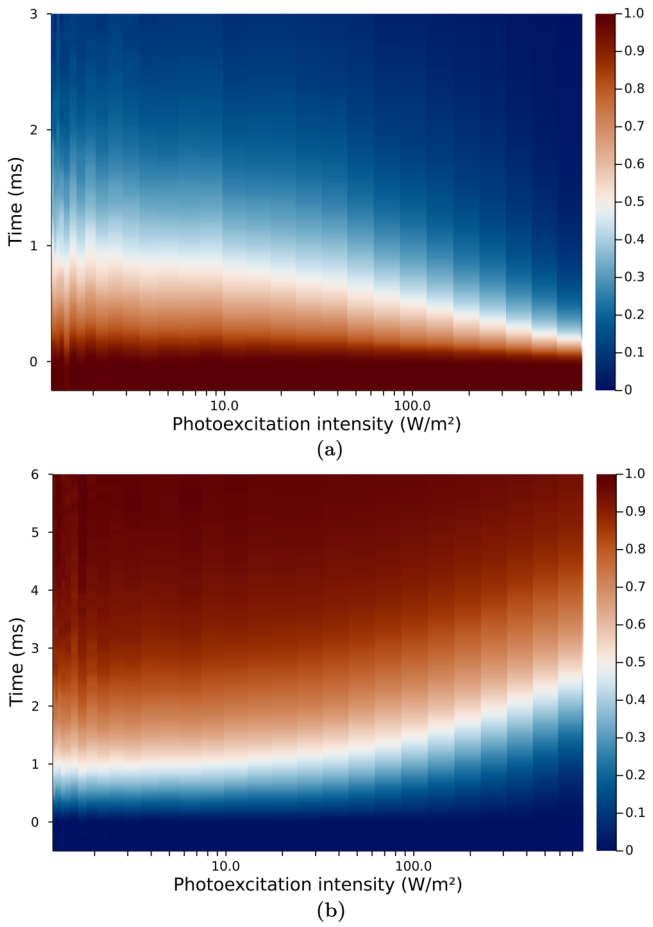

FIG. 3. The switch on (a) and switch off (b) dynamics of the transmission through area 5 of the partially passivated wafer as a function of the photoexcitation intensity. Here, photoexcitation is at the partially passivated surface. The transmission for each photoexcitation intensity is normalized to the maximum and minimum values so that the change in switching time as a function of the photoexcitation intensity can be easily observed. Results for all areas on the wafer can be found in the supplementary material (Sec. 2).

The extracted effective charge carrier lifetimes for each of the nine regions are plotted as a function of filling fraction in Fig. 5. The filling fractions of each region are measured from microscope images taken after development of the photoresist—see supplementary material (Sec. 3). Also shown in Fig. 5 are modeled filling fraction dependent lifetimes from Eqs. (1)–(3) for different SRVs of the unpassivated holes—the SRV of the passivated areas, and of the fully passivated surface, is taken to be 0.001 m s^{-1}. The modeling suggests that the SRV of the unpassivated holes is between 15 and 40 m s^{-1}. Figure 5 clearly demonstrates that by etching holes into a surface passivation layer, we can tune the effective charge carrier lifetime over a range that would otherwise not be achievable with standard uniform surface passivation schemes.

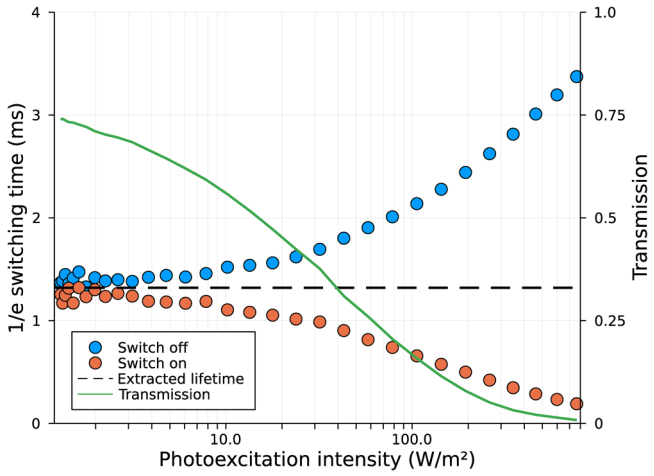

FIG. 4. Dots show the 1/e switch on and switch off times as a function of the photoexcitation intensity as extracted from the data presented in Fig. 3. Also shown is the intensity dependent steady-state transmission (after the photoexciting lamp had been turned on for a long period, green line), and the extracted effective charge carrier lifetime (black dashed line). Similar plots for each region can be found in the supplementary material (Sec. 2).

V. TRANSMISSION SWITCHING TIMES

The effective charge carrier lifetime is the average time that an excess charge carrier will exist before recombining, given here by the time it takes for the integrated excess carrier density to decrease to 1/e of its steady-state value upon switching off a photoexciting source. As discussed previously, for the range of carrier densities generated in this study, we expect a photoexcitation intensity

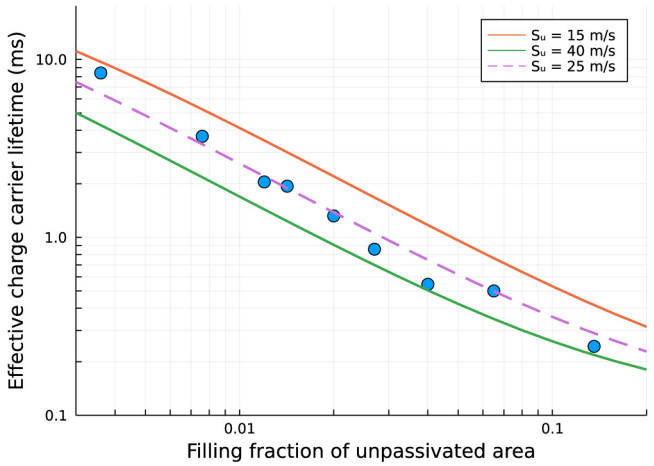

FIG. 5. Blue dots show the effective lifetimes vs filling fraction of the holes in the passivated layer extracted from the switching dynamics for each patterned area. The lines are results from our analytical model for different SRV values of the unpassivated holes, S_u, using Eqs. (1)–(3).

independent carrier lifetime to be a good approximation. Despite this, a somewhat unexpected observation from Figs. 3 and 4 is that the time-dynamics associated with switching on/off the transmission through the wafer are not solely dependent on this carrier lifetime; there is also a marked intensity dependence—for high photoexcitation intensities, the switch off dynamics are considerably slower than the switch on dynamics.

It is relatively simple to understand the root cause of this divergence of the switching times if we consider the limit as ΔT approaches T_0, i.e., complete blocking. In this limit, we can define an average carrier density through the wafer, Δn_e, that is required to reduce the transmission to T_0/e (the switch on time in this limit as defined previously). Any increase in photoexcitation intensity will reduce the time required to reach Δn_e, and thus the switch-on time will be correspondingly reduced. Conversely, if the photoexcitation intensity is such that the resulting carrier density is far beyond that required to essentially switch off all transmission through the wafer, there will be a delay as this excess of carriers recombine before the carrier density reduces sufficiently that transmission begins to increase. Thus, the divergence in switching times essentially arises due to the nonlinear variation, and subsequent saturation, of the transmission through a wafer as a function of carrier density.

While the divergence in switching times is simple to understand in this limit of ΔT approaching T_0, the details of the switching dynamics are a little more complex. However, before discussing this further, it will be useful to first consider the steady-state change in transmission upon photoexcitation. The equilibrium excess carrier density upon photoexcitation depends upon the carrier lifetime, and thus the change in transmission through the wafer would be expected to depend similarly. Indeed, we see this behavior in our data (e.g., by comparing the photoexcitation intensity dependent transmission for area 5, shown by the green solid line in Fig. 4, to similar results for the other areas in the supplementary material (Sec. 2). At the same time, in Ref. 13, we showed that the transmitted intensity also depends upon the thickness of the wafer, and crucially upon Fabry–Pérot resonances which occur when the wafer thickness is an integer multiple of half of a wavelength ($d = m\lambda_0/2n$, where λ_0 is the free-space wavelength and n is the refractive index of Si at λ_0). In Ref. 13, we have detailed a finite difference solver for calculating the steady-state charge carrier dynamics within a wafer upon photoexcitation, which, when combined with a Drude model for the dielectric permittivity profile, can be used to calculate the transmission of radiation through a photoexcited wafer. In Fig. 6(a), we show the normal incidence transmission of 321 GHz radiation as a function of wafer thickness for various excitation intensities, assuming 625 nm wavelength excitation light incident upon a wafer with a bulk lifetime of 50 ms, $S_0 = 0.5\,\mathrm{m\,s^{-1}}$ and $S_1 = 0.001\,\mathrm{m\,s^{-1}}$. The value of $0.5\,\mathrm{m\,s^{-1}}$ for S_0 mimics the value obtained using Eq. (3) for area 5 of our wafer. Thus, the data in Fig. 6(a) for a thickness of 670 μm approximate what one would expect for this region of our wafer. The vertical dashed line indicates the 670 μm wafer thickness used in our experiments—normally incident 321 GHz radiation is close to a Fabry–Pérot resonance, enhancing the modulation efficiency.

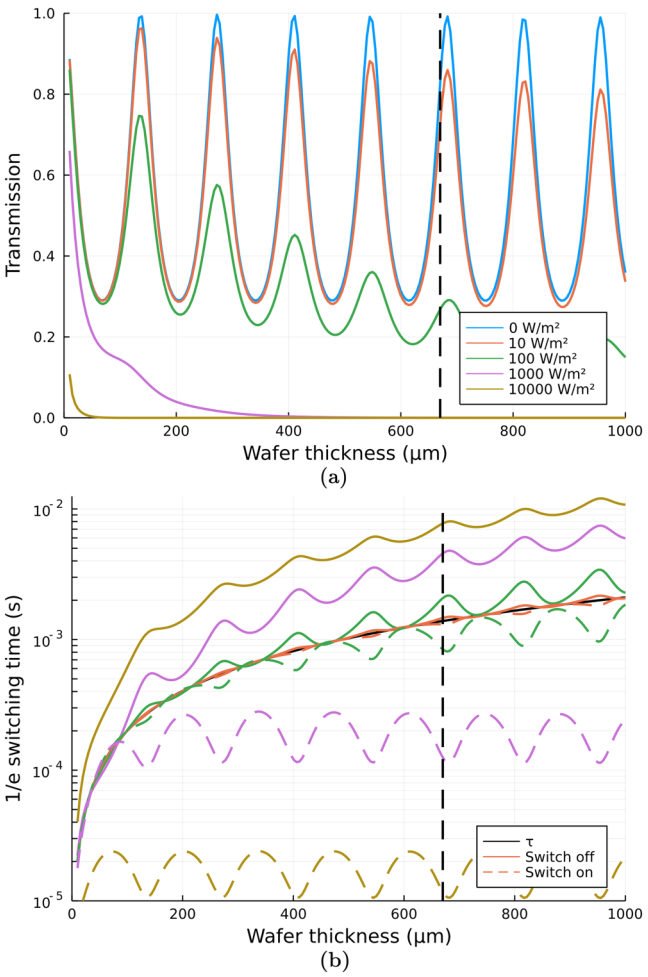

FIG. 6. The modeled transmission, (a), and 1/e switch on and switch off times, (b), as a function of wafer thickness for 321 GHz radiation incident upon a wafer with an effective surface recombination velocity of $0.5\,\mathrm{m\,s^{-1}}$ on the surface being photoexcited ("partially" passivated, corresponding to an unpassivated SRV of $S_u = 25\,\mathrm{m\,s^{-1}}$ and a hole fill fraction of 0.02, mimicking area 5 of our wafer), and $0.001\,\mathrm{m\,s^{-1}}$ on the opposite surface ("fully" passivated) for photoexcitation intensities of 0, 10, 100, 1000, and 10 000 $\mathrm{W\,m^{-2}}$. The black line represents the effective lifetime, τ as calculated from Eqs. (1) and (2). Vertical dashed line represents the wafer thickness used in our experiments.

Since the overall change in transmission upon photoexcitation depends upon these resonances within the thickness of the wafer, one might reason that the switching dynamics could similarly depend upon the thickness. In an extension to our finite difference solver, we calculate the time dynamics of the carrier density profile throughout the wafer upon switching on/off a generation rate. This extension is detailed in the supplementary material (Sec. 4), and here we have used it to calculate the time-dynamics of the normal incidence transmission of 321 GHz radiation through a wafer for the same parameters as for Fig. 6(a), allowing us to calculate the

switch on and switch off times as defined previously. The results of these calculations are shown in Fig. 6(b), alongside the effective charge carrier lifetime, τ, as calculated using Eqs. (1) and (2).

The first point to note is that the effective charge carrier lifetime, τ, increases with increasing wafer thickness. This is expected since the carrier lifetime is dominated by recombination at the surfaces as the probability per unit time of a diffusing charge carrier within the wafer encountering a surface is reduced in thicker wafers. For low excitation intensities [red and green curves in Fig. 6(b)], both switch on and switch off times lie close to the thickness-dependent carrier lifetime. However, as the excitation intensity increases [purple and brown lines in Fig. 6(b)], the carrier density increases and the transmission decreases, resulting in the divergence of the switch on and switch off times. This divergence is enhanced by the Fabry–Pérot resonances due to the increased light-matter interaction—the resonantly enhanced fields inside the silicon wafer result in greater absorption for a given change in conductivity, essentially making the transmission as a function of average carrier density more sub-linear.

Thus, we can conclude that, since it is the longer switching time that will determine a modulator's operational frequency, if one requires an efficient modulator with a maximal change in transmission it is the switch off time that will be the limiting factor.

VI. SUMMARY

We have designed a new type of silicon-based metamaterial with a tuneable electron-hole lifetime. By periodically patterning a dielectric passivation layer, we show that the effective charge carrier lifetime in Si can be tuned, resulting in carrier lifetimes of between 200 μs and 8 ms in a 670 μm thick Si wafer, though, in principle, any lifetime between the fully passivated and fully unpassivated limits could be achieved. We have further investigated the switching times of photomodulators with such intermediate charge carrier lifetimes, and have shown that they crucially depend upon the photoexcitation intensity and details of the carrier dynamics, as well as the carrier lifetime. As such, there is an inherent trade-off between achieving large modulation depths and fast switching times.

This work will facilitate research using photomodulators as programmable spatial and temporal modulators at sub-IR frequencies, where there is currently a lack of other suitable means to achieve this, while the ability to tune the charge carrier lifetime may be useful for other semiconductor devices.

SUPPLEMENTARY MATERIAL

See the supplementary material for details of the modeling methods, and additional background information and modeling.

ACKNOWLEDGMENTS

This work was supported by the Engineering and Physical Sciences Research Council (EPSRC) of the UK (Grant Nos. EP/S036466/1, EP/S036261/1, EP/W003341/1, EP/V047914/1, and EP/V037749/1) and by the EPSRC and QinetiQ via the TEAM-A Prosperity Partnership (EP/R004781/1). Ailish Wratten is funded by an EPSRC studentship (No. EP/R513374/1) and Tim Niewelt is funded by a Leverhulme Trust Research Project Grant (No. RPG-2020-377). The authors thank Dr. F.D. Heinz from the University of Freiburg for fruitful discussions on the charge carrier dynamics.

AUTHOR DECLARATIONS

Conflict of Interest

The authors have no conflicts to disclose.

Author Contributions

I. R. Hooper: Conceptualization (lead); Data curation (lead); Formal analysis (lead); Funding acquisition (supporting); Investigation (lead); Methodology (equal); Project administration (supporting); Software (lead); Visualization (lead); Writing – original draft (lead); Writing – review & editing (equal). **E. Khorani:** Investigation (equal); Methodology (equal); Writing – review & editing (supporting). **X. Romain:** Investigation (supporting). **L. E. Barr:** Investigation (equal). **T. Niewelt:** Formal analysis (supporting); Writing – review & editing (supporting). **S. Saxena:** Investigation (supporting). **A. Wratten:** Investigation (supporting); Methodology (supporting). **N. E. Grant:** Conceptualization (supporting); Methodology (supporting); Project administration (supporting); Supervision (supporting). **J. D. Murphy:** Conceptualization (supporting); Funding acquisition (equal); Project administration (equal); Supervision (equal); Writing – review & editing (supporting). **E. Hendry:** Funding acquisition (lead); Project administration (equal); Supervision (equal); Writing – review & editing (equal).

DATA AVAILABILITY

The data that support the findings of this study are openly available in the University of Exeter institutional repository (ORE) at https://ore.exeter.ac.uk/repository/handle/10871/131938, Ref. 44.

REFERENCES

[1]M. Rahm, J.-S. Li, and W. J. Padilla, "THz wave modulators: A brief review on different modulation techniques," J. Infrared, Millim., Terahertz Waves **34**, 1–27 (2013).
[2]Z. T. Ma, Z. X. Geng, Z. Y. Fan, J. Liu, and H. D. Chen, "Modulators for terahertz communication: The current state of the art," Research **2019**, 6482975 (2019).
[3]L. Wang, Y. Zhang, X. Guo, T. Chen, H. Liang, X. Hao, X. Hou, W. Kou, Y. Zhao, T. Zhou, S. Liang, and Z. Yang, "A review of THz modulators with dynamic tunable metasurfaces," Nanomaterials **9**, 965 (2019).
[4]P. K. Nayak, S. Mahesh, H. J. Snaith, and D. Cahen, "Photovoltaic solar cell technologies: Analysing the state of the art," Nat. Rev. Mater. **4**, 269–285 (2019).
[5]M. J. Kenney, M. Gong, Y. Li, J. Z. Wu, J. Feng, M. Lanza, and H. Dai, "High-performance silicon photoanodes passivated with ultrathin nickel films for water oxidation," Science **342**, 836–840 (2013).
[6]T. Rahman, A. To, M. E. Pollard, N. E. Grant, J. Colwell, D. N. R. Payne, J. D. Murphy, D. M. Bagnall, B. Hoex, and S. A. Boden, "Minimising bulk lifetime degradation during the processing of interdigitated back contact silicon solar cells," Prog. Photovolt.: Res. Appl. **26**, 38–47 (2018).
[7]A. Cuevas and D. Macdonald, "Measuring and interpreting the lifetime of silicon wafers," Sol. Energy **76**, 255–262 (2004).

[8]R. S. Bonilla, B. Hoex, P. Hamer, and P. R. Wilshaw, "Dielectric surface passivation for silicon solar cells: A review," Phys. Status Solidi A **214**, 1700293 (2017).
[9]N. E. Grant and J. D. Murphy, "Temporary surface passivation for characterisation of bulk defects in silicon: A review," Phys. Status Solidi RRL **11**, 1700243 (2017).
[10]J. Schmidt, R. Peibst, and R. Brendel, "Surface passivation of crystalline silicon solar cells: Present and future," Sol. Energy Mater. Sol. Cells **187**, 39–54 (2018).
[11]B. Steinhauser, T. Niewelt, A. Richter, R. Eberle, and M. C. Schubert, "Extraordinarily high minority charge carrier lifetime observed in crystalline silicon," Sol. RRL **5**, 2100605 (2021).
[12]T. Niewelt, B. Steinhauser, A. Richter, B. Veith-Wolf, A. Fell, B. Hammann, N. E. Grant, L. Black, J. Tan, A. Youssef, J. D. Murphy, J. Schmidt, M. C. Schubert, and S. W. Glunz, "Reassessment of the intrinsic bulk recombination in crystalline silicon," Sol. Energy Mater. Sol. Cells **235**, 111467 (2022).
[13]I. R. Hooper, N. E. Grant, L. E. Barr, S. M. Hornett, J. D. Murphy, and E. Hendry, "High efficiency photomodulators for millimeter wave and THz radiation," Sci. Rep. **9**, 18304 (2019).
[14]S. Busch, B. Scherger, M. Scheller, and M. Koch, "Optically controlled terahertz beam steering and imaging," Opt. Lett. **37**, 1391–1393 (2012).
[15]T. F. Gallacher, R. Sondena, D. A. Robertson, and G. M. Smith, "Optical modulation of millimeter-wave beams using a semiconductor substrate," IEEE Trans. Microwave Theory Tech. **60**, 2301–2309 (2012).
[16]C. Rizza, A. Ciattoni, F. De Paulis, E. Palange, A. Orlandi, L. Columbo, and F. Prati, "Reconfigurable photoinduced metamaterials in the microwave regime," J. Phys. D: Appl. Phys. **48**, 135103 (2015).
[17]M. I. B. Shams, Z. Jiang, S. M. Rahman, L.-J. Cheng, J. L. Hesler, P. Fay, and L. Liu, "A 740-GHz dynamic two-dimensional beam-steering and forming antenna based on photo-induced reconfigurable Fresnel zone plates," IEEE Trans. Terahertz Sci. Technol. **7**, 310–319 (2017).
[18]D. F. Sievenpiper, J. H. Schaffner, H. J. Song, R. Y. Loo, and G. Tangonan, "Two-dimensional beam steering using an electrically tunable impedance surface," IEEE Trans. Antennas Propag. **51**, 2713–2722 (2003).
[19]T. J. Cui, M. Q. Qi, X. Wan, J. Zhao, and Q. Cheng, "Coding metamaterials, digital metamaterials and programmable metamaterials," Light: Sci. Appl. **3**, e218 (2014).
[20]H. Yang, X. Cao, F. Yang, J. Gao, S. Xu, M. Li, X. Chen, Y. Zhao, Y. Zheng, and S. Li, "A programmable metasurface with dynamic polarization, scattering and focusing control," Sci. Rep. **6**, 35692 (2016).
[21]L. Li, T. Jun Cui, W. Ji, S. Liu, J. Ding, X. Wan, Y. Bo Li, M. Jiang, C.-W. Qiu, and S. Zhang, "Electromagnetic reprogrammable coding-metasurface holograms," Nat. Commun. **8**, 197 (2017).
[22]Q. He, S. Sun, and L. Zhou, "Tunable/reconfigurable metasurfaces: Physics and applications," Research **2019**, 1849272 (2019).
[23]R. I. Stantchev, B. Sun, S. M. Hornett, P. A. Hobson, G. M. Gibson, M. J. Padgett, and E. Hendry, "Noninvasive, near-field terahertz imaging of hidden objects using a single-pixel detector," Sci. Adv. **2**, e1600190 (2016).
[24]Q. Sun, X. Chen, X. Liu, R. I. Stantchev, and E. Pickwell-MacPherson, "Exploiting total internal reflection geometry for terahertz devices and enhanced sample characterization," Adv. Opt. Mater. **8**, 1900535 (2020).
[25]R. I. Stantchev, X. Yu, T. Blu, and E. Pickwell-MacPherson, "Real-time terahertz imaging with a single-pixel detector," Nat. Commun. **11**, 2535 (2020).
[26]L. E. Barr, P. Karlsen, S. M. Hornett, I. R. Hooper, M. Mrnka, C. R. Lawrence, D. B. Phillips, and E. Hendry, "Super-resolution imaging for sub-IR frequencies based on total internal reflection," Optica **8**, 88–94 (2021).
[27]Y. He, Y. Wang, M. Li, Q. Yang, Z. Chen, J. Zhang, and Q. Wen, "All-optical spatial terahertz modulator with surface-textured and passivated silicon," Opt. Express **29**, 8914–8925 (2021).
[28]L. E. Black, *New Perspectives on Surface Passivation: Understanding the Si-Al_2O_3 Interface* (Springer International Publishing, 2016).
[29]G. Dingemans and W. M. M. Kessels, "Status and prospects of Al_2O_3-based surface passivation schemes for silicon solar cells," J. Vac. Sci. Technol. A **30**, 040802–28 (2012).
[30]G. Agostinelli, A. Delabie, P. Vitanov, Z. Alexieva, H. F. W. Dekkers, S. De Wolf, and G. Beaucarne, "Very low surface recombination velocities on p-type silicon wafers passivated with a dielectric with fixed negative charge," Sol. Energy Mater. Sol. Cells **90**, 3438–3443 (2006).
[31]*Semiconductor Module User's Guide* (COMSOL AB, Stockholm, 2021); available at https://doc.comsol.com/6.1/doc/com.comsol.help.semicond/SemiconductorModuleUsersGuide.pdf.
[32]F. D. Heinz, W. Warta, and M. C. Schubert, "Separation of the surface and bulk recombination in silicon by means of transient photoluminescence," Appl. Phys. Lett. **110**, 042105 (2017).
[33]D. K. Schroder, *Semiconductor Material and Device Characterization* (John Wiley & Sons, 2015).
[34]A. Sproul, "Dimensionless solution of the equation describing the effect of surface recombination on carrier decay in semiconductors," J. Appl. Phys. **76**, 2851–2854 (1994).
[35]Y.-I. Ogita, "Bulk lifetime and surface recombination velocity measurement method in semiconductor wafers," J. Appl. Phys. **79**, 6954–6960 (1996).
[36]G. Dingemans, R. Seguin, P. Engelhart, M. C. M. van de Sanden, and W. M. M. Kessels, "Silicon surface passivation by ultrathin Al_2O_3 films synthesized by thermal and plasma atomic layer deposition," Phys. Status Solidi RRL **4**, 10–12 (2010).
[37]S. L. Pain, E. Khorani, T. Niewelt, A. Wratten, G. J. Paez Fajardo, B. P. Winfield, R. S. Bonilla, M. Walker, L. F. J. Piper, N. E. Grant, and J. D. Murphy, "Electronic characteristics of ultra-thin passivation layers for silicon photovoltaics," Adv. Mater. Interfaces **9**, 2201339 (2022).
[38]N. E. Grant, V. P. Markevich, J. Mullins, A. R. Peaker, F. Rougieux, and D. Macdonald, "Thermal activation and deactivation of grown-in defects limiting the lifetime of float-zone silicon," Phys. Status Solidi RRL **10**, 443–447 (2016).
[39]N. E. Grant, V. P. Markevich, J. Mullins, A. R. Peaker, F. Rougieux, D. Macdonald, and J. D. Murphy, "Permanent annihilation of thermally activated defects which limit the lifetime of float-zone silicon," Phys. Status Solidi A **213**, 2844–2849 (2016).
[40]T. Trupke, R. A. Bardos, M. C. Schubert, and W. Warta, "Photoluminescence imaging of silicon wafers," Appl. Phys. Lett. **89**, 044107 (2006).
[41]The source consisted of a Linwave LW22-797599 107 GHz Gunn oscillator with a Virginia Diodes frequency tripler and diagonal horn antenna.
[42]The detector was formed from an RPG SHM300 sub-harmonic mixer with horn antenna and LO source (a frequency doubled RPG 80 GHz Gunn diode source), which downconverts the detected signal for detection with an HP 8473B.01-18 GHz coaxial detector.
[43]W. S. Cleveland and E. Grosse, "Computational methods for local regression," Stat. Comput. **1**, 47–62 (1991).
[44]I. R. Hooper, E. Khorani, X. Romain, L. E. Barr, T. Niewelt, S. Saxena, A. Wratten, N. E. Grant, J. D. Murphy, and E. Hendry, "Engineering the carrier lifetime and switching speed in Si-based mm wave photomodulators," ORE (2022). https://ore.exeter.ac.uk/repository/handle/10871/131938